Published in Journal of Electroanalytical Chemistry 560, issue 1, 47-56, 2006
which should be used for any reference to this work

Theoretical treatment and computer simulation of microelectrode arrays

Werner E. Morf *, Milena Koudelka-Hep, Nicolaas F. de Rooij

SAMLAB, Institute of Microtechnology (IMT), University of Neuchâtel, Rue Jaquet-Droz 1, CH-2007 Neuchâtel, Switzerland

Abstract

New relations for and interrelations between the current responses of different microelectrode arrays are presented. Interdigitated microelectrode arrays (IDAs: alternating cathodes and anodes) and uniform microband electrode arrays (MEAs: only cathodes or anodes) are treated, and miniaturized systems with planar band electrodes or hemicylinder electrodes are discussed. A common basis was found for the specific response characteristics of IDAs and MEAs. The theoretical expressions were verified by results from computer modelling. The numerical simulations made use of finite-element procedures to evaluate steady-state and time-dependent mass fluxes and concentration profiles of electroactive species at the surfaces of different microelectrode arrays. It was shown that the response behavior of a given array can be exactly predicted from the current data of other arrays.

Keywords: Microelectrodes; Interdigitated electrode array; Current response; Concentration profiles; Theory; Computer simulation; Finite-element method

1. Introduction

The fundamental understanding and the reliable prediction of diffusional interactions between microelectrodes is a prerequisite for the tailored design of microelectrode arrays. Based on this knowledge, the design criteria of microelectrode arrays can be optimized in view of selected applications. For example, the inter-electrode gap can be adapted either for enhancing or for reducing the diffusional coupling between the electrodes.

Besides the regular microdisk arrays, the arrays of uniform microband electrodes and of interdigitated microelectrodes are the most common configurations. For both classes of electrode arrays, theoretical or semi-quantitative treatments as well as computer simulations have been developed by several groups in order to study the influence of geometrical parameters on the diffusion fluxes.

Already in 1986, Bard et al. treated the diffusional mass transfer to a single microband electrode and to a closely spaced microband array [1]. By digital simulation, they demonstrated the preponderate influence of the gap size on the collection efficiency. Conformal maps for modelling the collector–generator behavior as a function of the width-to-gap ratio for a double [2] and a triple band configuration [3] have shown a good agreement between models and experimental data. Later, the application-specific modelling based on conformal mapping was successfully adopted for simulating the current distribution at dual microband electrodes and their efficiency in electrochemical titrations [4,5]. A diffusion model was also exploited for characterizing the flow rates in microchannels [6]. Most of these treatments can only be considered as semi-quantitative descriptions. However, an exact theory of the steady-state mass fluxes at interdigitated planar microelectrode arrays was contributed by Aoki et al. [7].

The interdigitated arrays are mainly applied in a three-electrode cell with an external counter electrode (e.g., a platinum wire), and a generation-collection mode is used to improve, due to the redox cycling, the electroanalytical sensitivity and the detection limits [1]. Therefore, the relationship between the geometrical parameters of

* Corresponding author. Tel.: +41 32 720 52 34; fax: +41 32 720 57 11.
E-mail address: werner.morf@unine.ch (W.E. Morf).

the interdigitated microelectrode arrays and the redox cycling efficiency has been extensively investigated in both stationary [8–10] and flow systems [11–13].

The present contribution aims at a more fundamental understanding of the specifications of and the interrelations between different electrode arrays. Thus, we focus on the amperometric and chronoamperometric response behavior of interdigitated microelectrode arrays (IDAs: alternating cathodes and anodes) and uniform microelectrode arrays (MEAs: only cathodes or anodes). The diffusion-controlled currents at IDAs and MEAs are treated theoretically for miniaturized arrays based on planar band electrodes and hemicylinder electrodes, respectively. A common basis for the specific characteristics of IDAs and MEAs is found from the principles of superimposition of diffusion fluxes. The theoretical expressions are verified by computer modelling using finite-element procedures. This leads to a deeper insight into the response behavior of electrode arrays.

2. Theory

2.1. Current response of symmetrical IDAs without external counter electrodes

The amperometric response of IDAs based on parallel planar microband electrodes was treated theoretically by Aoki et al. [7,14,15]. The exact solution derived for the current flow at steady state may be written as [7]:

$$i_{el}\,(\mathrm{IDA}) = \pm nFDC^0.\alpha L_{el} \quad \text{(band electrodes)}, \tag{1}$$

$$\alpha = 4K(1-p)/K(p), \tag{2}$$

where i_{el} is the diffusion-limited current at a single cathode or anode of the array (sign + or − in Eq. (1)), n is the charge number involved, F is the Faraday equivalent, D is the diffusion coefficient assumed to be the same for all reacting species, C^0 is the bulk concentration of the decisive species, L_{el} is the electrode length, and α is a dimensionless function given by the ratio of complete elliptic integrals, $K(1-p)$ and $K(p)$, where p depends on the width of the electrodes and on the inter-electrode distance. For IDAs with cathodes and anodes of the same width w_{el}, separated by gaps of the width w_g, the parameter p is defined by [7]:

$$p = 4\sin(\pi w_g/2w)/(1+\sin(\pi w_g/2w))^2, \quad w = w_{el} + w_g, \tag{3}$$

where w is the distance between the central axes of two neighbouring electrodes.

Aoki et al. [7] described α by the series expression in Eq. (4) which, however, turns out to be useful only for extreme cases with $p \leqslant 0.5$ and hence $w_g \leqslant 0.1\ w_{el}$:

$$\alpha = -(4/\pi)\cdot\ln[(p/16) + 8(p/16)^2 + 84(p/16)^3 + 992(p/16)^4 + \cdots]. \tag{4}$$

For most relevant cases, the alternative formulation given in Eq. (5) is more adequate since it immediately converges for $p \geqslant 0.5$ and $w_g \geqslant 0.1 w_{el}$, respectively:

$$\alpha = -4\pi/\ln[(q/16) + 8(q/16)^2 + 84(q/16)^3 + 992(q/16)^4 + \cdots], \tag{5}$$

$$q = 1 - p = \tan^4(\pi w_{el}/4w). \tag{6}$$

A further reduction is possible for $w_g \geqslant w_{el}$, leading to the approximation:

$$\alpha \approx \pi/\ln(8w/\pi w_{el}). \tag{7}$$

Finally, the steady-state current response of the microband electrode array can be approximated by Eq. (8), which yields favourable results (see below):

$$i_{el}\,(\mathrm{IDA}) \approx \pm nFDC^0\cdot\pi L_{el}/ln(8w/\pi w_{el}) \quad \text{(planar electrodes)}. \tag{8}$$

A nearly identical relationship was derived earlier for an array of so-called line electrodes, which are very thin hemicylinder electrodes of radius r_{el} (see appendix of Ref. [16]):

$$i_{el}\,(\mathrm{IDA}) = \pm nFDC^0\cdot\pi L_{el}/\ln(2w/\pi r_{el}) \quad \text{(hemicylindrical electrodes)}. \tag{9}$$

It should be mentioned that systems with hemicylinder electrodes are of more theoretical interest because they have not been realized so far. However, they are quoted here as a reference system for comparison.

2.2. Current response of uniform MEAs versus external counter electrodes

The current response of arrays that consist of uniform hemicylindrical line electrodes was described earlier (see appendix of Ref. [16]):

$$i_{el}\,(\mathrm{MEA}) = \pm nFDC^0\cdot L_{el}/[\pi^{-1}\ln(w/2\pi r_{el}) + \delta_N/w] \quad \text{(hemicylindrical electrodes)}, \tag{10}$$

where i_{el} is the steady-state current per electrode of length L_{el} and radius r_{el} (the sign + is used for cathodes, and the sign − for anodes), w is the interelectrode distance, and δ_N is the average thickness of the Nernstian diffusion layer arising between the array and the bulk solution. This layer is defined in the classical sense as the hypothetical stagnant diffusion layer formed at steady state [17]. Accordingly, δ_N is directly related to the hydrodynamic boundary layer and is controlled by the extent of natural or forced convection in the solution. Evidently, the Nernstian layer thickness sets an upper limit to the diffusion length, $\delta_t = \sqrt{(\pi Dt)}$, which enters in time-dependent descriptions of mass transport to electrodes [17] (see also below).

Quite an analogous expression may be established for arrays of uniform planar microband electrodes of width w_{el}. When replacing r_{el} in Eq. (10) by $w_{el}/4$, as for Eqs. (8) and (9), the following approximation is obtained:

$$i_{el}\ (\mathrm{MEA}) = \pm nFDC^0 \cdot \beta L_{el} \quad \text{(planar electrodes)}, \tag{11}$$

$$\beta \approx [\pi^{-1} \ln(2w/\pi w_{el}) + \delta_N/w]^{-1}. \tag{12}$$

It will be shown that this result permits a nearly perfect fit of current data for MEAs.

A comparison of Eqs. (8)–(12) makes evident that a close relationship exists between the responses of IDAs and MEAs. As a matter of fact, any IDA (with $w = w_o$) can be constructed hypothetically from superimposition of a MEA of identical geometries ($w = w_o$) that only contains anodes, and a doubly spaced MEA ($w = 2w_o$) that exclusively consists of doubly polarized cathodes. This offers an explanation for the fundamental new relationship that can be derived from Eqs. (8)–(12):

$$i_{el}^{-1}\ (\mathrm{IDA}, w = w_o) \approx 2i_{el}^{-1}\ (\mathrm{MEA}, w = 2w_o) - i_{el}^{-1}\ (\mathrm{MEA}, w = w_o), \tag{13}$$

respectively

$$\alpha^{-1}\ (w = w_o) \approx 2\beta^{-1}\ (w = 2w_o) - \beta^{-1}\ (w = w_o). \tag{14}$$

It is highly remarkable that exactly the same interdependence as in Eq. (13) applies when IDAs and MEAs are used in chronoamperometric or similar non-steady-state experiments, as will be shown later.

2.3. Current response of IDAs versus external counter electrodes

The former description of the current response of IDAs relies on the steady-state condition [7] that the involved electroactive species (oxidized (O) or reduced (R)) show 'symmetrical' concentration profiles according to the following equations:

$$C_O^c + C_O^a = 2C_O^0, \quad C_R^c + C_R^a = 2C_R^0 \tag{15}$$

$$C_O^0 - C_O^c = C_R^0 - C_R^a, \tag{16}$$

where C^c and C^a are the boundary concentrations of O or R at the cathodes and the anodes, respectively, and C^0 are the corresponding bulk concentrations. Obviously, the simultaneous presence of both species in the bulk solution is needed to fulfill the requirements for a steady-state current flow:

$$i_{el}\ (\mathrm{IDA}) = \pm nFD(C_O^0 - C_O^c) \cdot \alpha L_{el} = \pm nFD(C_R^0 - C_R^a) \cdot \alpha L_{el}. \tag{17}$$

Symmetrical concentration profiles are found to be a prerequisite for the equivalence of cathodic and anodic currents. Limiting currents according to Eq. (1) are reached if either $C_O^c \to 0$ (for $C_R^0 \geqslant C_O^0$) or $C_R^a \to 0$ holds (for $C_O^0 \geqslant C_R^0$).

A different situation is encountered when the cathodes and the anodes of IDAs are driven separately versus external counter electrodes. In this case, the average concentrations near the electrodes, $C^* = 0.5\ (C^c + C^a)$, usually deviate from the bulk values C^0. Hence, the relations given in Eqs. (15) and (16) have to be replaced by:

$$C_O^c + C_O^a = 2C_O^*, \quad C_R^c + C_R^a = 2C_R^* \tag{18}$$

$$C_O^* - C_O^c = C_R^* - C_R^a, \tag{19}$$

where $C_O^* + C_R^* = C_O^0 + C_R^0$ holds. The concentration differences $C^0 - C^*$ give rise to additional diffusion currents that contribute to the total response of the electrodes:

$$\begin{aligned} i_{el}\ (\mathrm{IDA\ vs.\ CE}) &= \pm nFD(C_O^* - C_O^c) \cdot \alpha L_{el} \\ &\quad + nFD(C_O^0 - C_O^*) \cdot \beta L_{el} \\ &= \pm nFD(C_R^* - C_R^a) \cdot \alpha L_{el} \\ &\quad - nFD(C_R^0 - C_R^*) \cdot \beta L_{el}, \end{aligned} \tag{20}$$

where the first terms are positive for cathodes and negative for anodes. The derivation of Eq. (20) obviously makes use of a superimposition of the diffusion models for a conventional IDA without external electrode (first term) and for a MEA (second term). The theoretical basis of such procedures for the solution of diffusion problems is extensively discussed in Crank's work [18] and will not be repeated here. However, a convincing illustration of the superimposition principle will be given in Section 3, where the additivity of concentration profiles for different electrode arrays is demonstrated.

Evidently, Eq. (20) constitutes the most general description of the steady-state response behavior exhibited by electrode arrays since it covers all cases treated before. For IDAs coupled to external electrodes, as a rule, the equivalence of cathodic and anodic currents at the array electrodes is usually no longer maintained. In fact, the second terms in Eq. (20) account for the external net current flow. The limiting currents obtained for $C_O^c \to 0$ as well as $C_R^a \to 0$ can finally be described by:

$$\begin{aligned} i_{el}\ (\mathrm{IDA\ vs.\ CE}) &= \pm nFD(C_O^0 + C_R^0) \cdot 0.5\alpha L_{el} \\ &\quad + nFD(C_O^0 - C_R^0) \cdot 0.5\beta L_{el}. \end{aligned} \tag{21}$$

This response function clearly deviates from the former equation (1). The only exception is found for an IDA that is exposed to a 1:1 mixture of O and R. Here, the second term in Eq. (21) is eliminated and the description is reduced to Eq. (1) with $C^0 = C_O^0 = C_R^0$. In all other cases, the use of external counter electrodes changes the current behavior of IDAs considerably. For example, the response to a pure solution of O (with $C_O^0 = C^0$ and $C_R^0 = 0$) is given by:

$$i_{el}\ (\text{IDA-cathode vs. CE}) = +nFDC^0 \cdot \gamma_1 L_{el} \quad \text{with } \gamma_1 = 0.5(\alpha + \beta), \tag{22a}$$

$$i_{el}\ (\text{IDA-anode vs. CE}) = -nFDC^0 \cdot \gamma_2 L_{el} \quad \text{with } \gamma_2 = 0.5(\alpha - \beta), \tag{22b}$$

where the ratio of the coefficients γ_1 and γ_2 is comparable (but not identical) to the collection efficiency of IDAs observed in dynamic measurements [1]. Apparently, the response parameters do not only depend on the geometry of the array but also on its mode of operation, and they are even influenced by the composition of the aqueous solution. These predictions are confirmed by both steady-state and

time-dependent results from numerical simulations of IDAs, as described in the following.

2.4. Computer simulation of electrode arrays

Numerical simulations of the current distribution at different microband electrode arrays (IDAs and MEAs) are a suitable approach for verifying the theoretical results derived before. In fact, the computer modelling of the underlying diffusion processes can be considered as a sort of numerical experiment. A finite-element method is found to be a favourable choice, especially since in the present case the calculations are greatly simplified due to the specific conditions. The full details of the procedure are given in Appendix A. Results of these model calculations are presented and discussed in the next section.

3. Results and discussion

3.1. Studies on IDAs without external counter electrodes

To analyze the current response of IDAs based on microband electrodes, the underlying diffusion processes were studied using computer simulations (see Appendix A). Finite-element procedures based on the following parameters were generally applied. The unit cell contained two half-electrodes of the same width and an intermediate gap of variable width, and its range in y-direction covered the average Nernstian diffusion layer. Unless otherwise specified, the electrode width extended over 10 elements and the diffusion layer over 98 elements. For simplicity, it was assumed that $C_O^0 = C_R^0$ holds, so that Eq. (1) can be applied with either of the two concentrations for comparison. All calculations were performed with conventional MS Excel software (Microsoft Corporation).

Results obtained for several IDAs that differ in the gap width are summarized in Table 1. The values α found from the computer simulations are compared with theoretical values according to Eqs. (5) and (7). Evidently, there is a very close agreement between the numerical results determined from the finite-element method and the exact values based on Eq. (5), the relative deviations being $\leqslant 1\%$ throughout. This clearly confirms that the present computer simulations are capable of a quite realistic modelling of diffusion processes at electrode arrays. Furthermore, the good correlation can be considered as a final proof for the validity of the theoretical equations. Table 1 includes also some information on the quality of the approximation given in Eq. (7). As a rule, the deviations from the exact results according to Eq. (5) are $\leqslant 1\%$ for IDAs with $w_g > w_{el}$, but up to 8% for very close arrays of electrodes.

Table 1
Values α of the current response in Eq. (1) for IDAs in symmetrical arrangements[a]

w/w_{el}	α (finite-element)	α (Eq. (5))	α (Eq. (7))
1.5	2.564	2.559	2.344
2	1.984	2.000	1.930
	1.984[b]	2.000[b]	1.930[b]
	1.976[c]		
3	1.548	1.563	1.545
4	1.348	1.361	1.354

[a] Details on the calculations and on the parameters used are given in the text.
[b] For a diffusion layer of 58 instead of 98 elements (i.e., $\delta_N/w_{el} = 5.8$).
[c] For an electrode width of 2×10 elements and a diffusion layer of 2×58 elements.

Calculations were also performed for a given system using a different thickness of the Nernstian diffusion layer or a larger number of finite elements per electrode width (Table 1). The results clearly confirm that the diffusion layer has actually no influence on the value α, as is expected from theory (see Eqs. (5) and (7)). This implies, of course, that the current response is here completely independent of any convection influences in the bulk solution. It should however be mentioned that this is only true for IDAs with $\delta_N \gg 0.5\ w_g$. An even more important issue is that the results for α are found to be nearly insensitive to the number of elements chosen per unit cell. Obviously, computations using a finer-meshed grid of elements do not bear any advantages. Thus, the usual procedure with 10 elements per electrode width turns out to be near the optimum.

Fig. 1 illustrates the steady-state concentration profiles for oxidized and reduced species near the array electrodes. The whole solution range shown corresponds to about one third of the Nernstian layer. The profiles for O and R are found to be perfectly symmetrical, which agrees with the expectations for an IDA when no external electrodes are involved. Evidently, significant gradients of the concentrations are restricted to a very thin boundary zone the thickness of which is comparable to the interelectrode distance. Virtually no gradients arise between this region and the bulk solution.

3.2. Studies on uniform MEAs versus external counter electrodes

Computer simulations were also made for uniform microband electrode arrays in contact with a bulk solution of O, i. e., with $C_O^0 = C^0$ and $C_R^0 = 0$. In Table 2, the derived numerical values β are compared with the ones quoted from Eq. (12). Surprisingly, a nearly perfect correlation between the two sets of data is found. In fact, the relative deviations are $<1\%$ throughout. This documents both the capability of the numerical method and the applicability of the theoretical expression introduced in this work.

According to Table 2, the current response of MEAs depends on the thickness of the Nernstian diffusion layer. This observation clearly contrasts with the former findings for IDAs (see Table 1). However, the specific behavior of MEAs is predicted by Eqs. (11) and (12) and is also confirmed by the results of the computer modelling. The agreement between theory and numerical simulation is again excellent. The observed increase of β with increasing

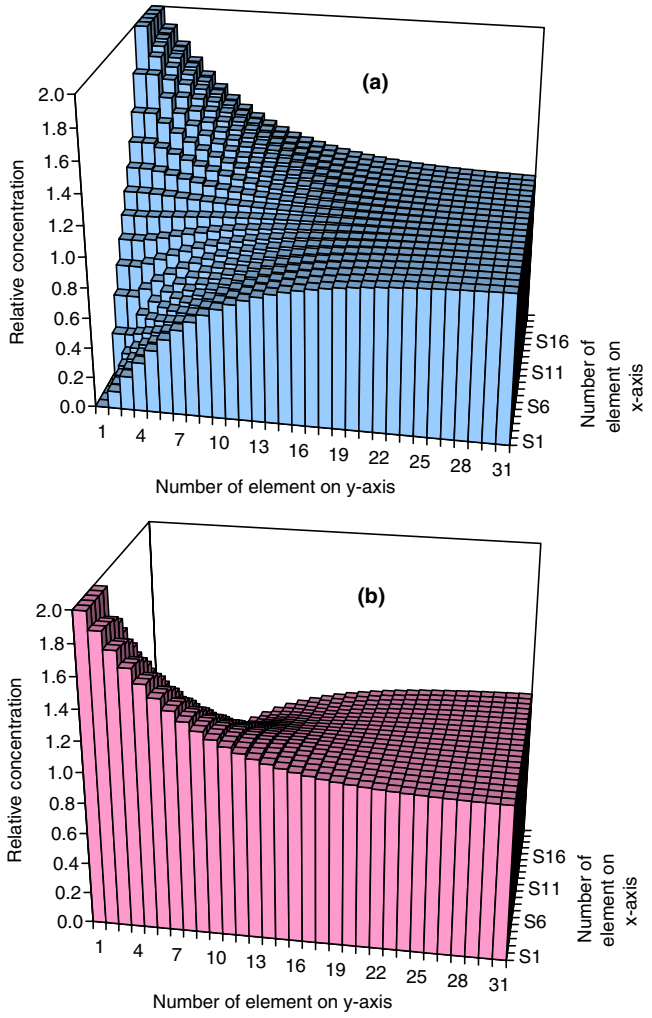

Fig. 1. Concentration profiles for oxidized species O (a) and reduced species R (b) near the surface of an interdigitated electrode array (IDA) without external counter electrode. Steady-state concentrations in units of C^0 are shown for a solution area that is confined in x-direction by the centres of a cathode (front axis on the left side) and a neighbouring anode (back axis on the left side) and extends in y-direction to ~30% of the Nernstian layer separating the electrodes from the bulk solution. The values were obtained from finite-element calculations with 10 elements per electrode width, using $w_g = w_{el}$, $\delta_N = 9.8$ w_{el} and $C_O^0 = C_R^0 = C^0$. For electrodes of 5 μm width, the shown x–y-area corresponds to 10 μm × 15 μm.

Table 2
Values β of the current response in Eq. (11) for MEAs versus external electrodes[a]

w/w_{el}	β (finite-element)	β (Eq. (12))
1.5	0.152	0.153
2	0.200	0.201
	0.334[b]	0.336[b]
3	0.287	0.288
4	0.363	0.364
	0.571[b]	0.572[b]

[a] Details on the calculations and on the parameters used are given in the text.
[b] For a diffusion layer of 58 instead of 98 elements (i.e., $\delta_N/w_{el} = 5.8$).

w/w_{el} is mainly due to the diffusion-layer-dependent term on the right-hand side of Eq. (12).

The data in Table 2 can also be used for verifying the interrelationship between the responses of IDAs and MEAs, as described in Eqs. (13) and (14). From the values β determined by the finite-element method for MEAs, one calculates $\alpha = 2.56$ and 1.96 for IDAs with $w/w_{el} = 1.5$ and 2, respectively. In the second case, the value $\alpha = 1.97$ is obtained from the data for systems with a reduced diffusion layer. These results are nearly identical with the true values given in Table 1.

Concentration profiles for the species O and R near the surface of a MEA are illustrated in Fig. 2. Again, the concentration distributions are fully symmetrical as for the IDA system in Fig. 1. In contrast to the former case, however, the present profiles exhibit pronounced gradients in the whole range shown. The reason is that a net mass transport by diffusion through the Nernstian layer is required

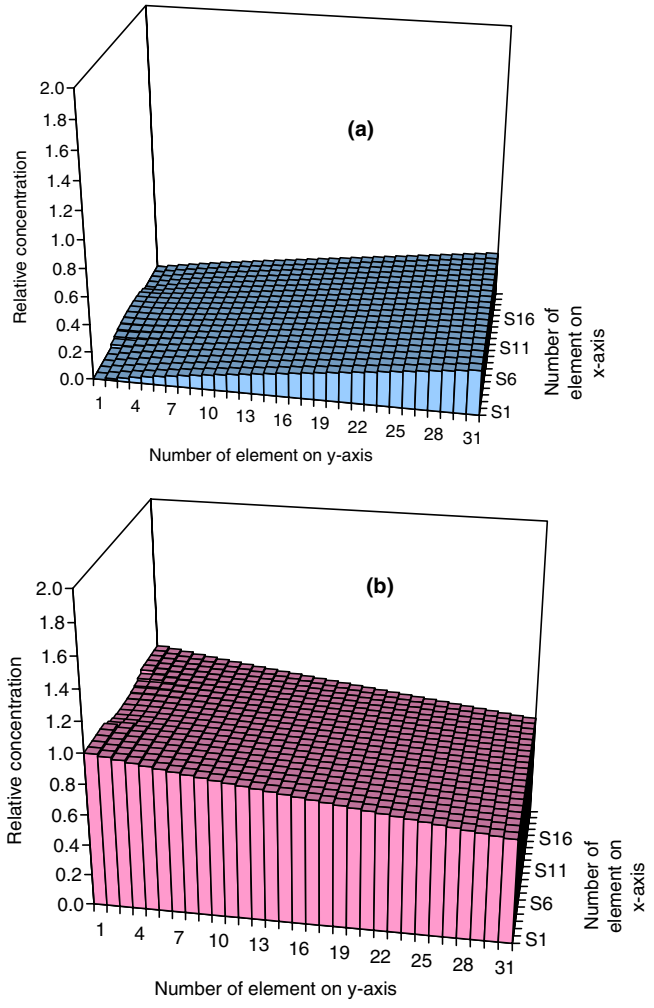

Fig. 2. Concentration profiles for species O (a) and R (b) at a uniform microband electrode array (MEA) coupled to an external electrode. Steady-state concentrations in units of C^0 are shown for an area between the centres of two neighbouring cathodes (front and back axis on the left side) and extending towards the bulk solution ($C_O^0 = C^0$, $C_R^0 = 0$). Further details are given in Fig. 1.

here to maintain a current flow between the IDA and the external counter electrode.

3.3. Studies on IDAs versus external counter electrodes

In this section, some results are given on the response behavior of IDAs when the current values at the cathodes and the anodes are measured separately versus external electrodes. The numerical simulations were made for electrode arrays exposed to a pure solution of oxidized species O. Table 3 contains some data on the coefficients γ_1 and γ_2 that are decisive for the current response of cathodes and anodes, respectively. It becomes evident that the results obtained from the finite-element procedure are completely identical with the ones based on Eq. (22). Although this may appear as a fortuitous coincidence at first sight, it finally turns out to be a proof for the strictly valid principle of superimposition of diffusion processes. The results clearly demonstrate that the current flows at the cathodes and the anodes of an IDA can differ considerably (here by up to 50%) as soon as external electrodes are involved.

Fig. 3 shows the steady-state concentration distributions of species O and R for the present case of an IDA. The profiles near the electrodes are quite similar to the ones depicted in Fig. 1, but the gradients towards the bulk solution rather resemble those in Fig. 2. These analogies are easily explained by the fact that the concentration values in Fig. 3 actually correspond to the exact sum of the values in Figs. 1 and 2. This perfect additivity of concentration profiles was fully confirmed for the studied system.

3.4. Results for the time response of IDAs and MEAs

The studies reported in the preceding sections focused on the steady-state current response of microband electrode arrays. In the numerical simulations, this final state was approximated by exposing the finite-element system to a large number of subsequent quasi-differential step changes with time. This implies that the computer modelling is not restricted to steady-state investigations but can also be used for analyzing the chronoamperometric response behavior. Similar studies on the time-dependent current characteristics of electrode arrays were reported by Aoki et al. [14,15].

Table 3
Values γ of the current response in Eq. (22) for IDAs versus external electrodes[a]

w/w_{el}	$\gamma_{1,2}$ (finite-element)		$0.5\ \alpha \pm 0.5\beta$ (finite-element[b])	
1.5	1.358	1.206	1.358	1.206
2	1.092	0.892	1.092	0.892
	1.159[c]	0.825[c]	1.159[c]	0.825[c]
3	0.917	0.630	0.917	0.630

[a] Details on the calculations and on the parameters used are given in the text.
[b] From computer simulations of symmetrical IDAs and MEAs.
[c] For a diffusion layer of 58 instead of 98 elements (i. e., $\delta_N/w_{el} = 5.8$).

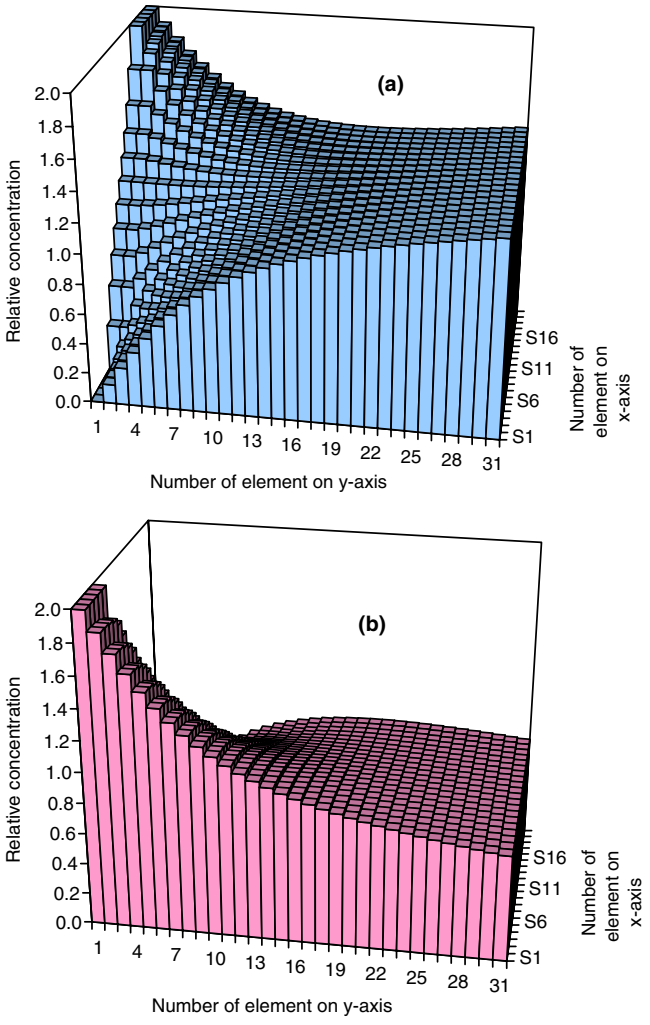

Fig. 3. Concentration profiles for species O (a) and R (b) at an IDA coupled to an external counter electrode. Steady-state concentrations in units of $0.5C^0$ are shown for an area between the centres of two neighbouring electrodes (front and back axis on the left side) and extending towards the bulk solution ($C_O^0 = C^0$, $C_R^0 = 0$). Further details are given in Fig. 1. (a) Obtained by superimposition of Figs. 1a and 2a.

Results on the chronoamperometric response are illustrated in Fig. 4 for IDAs, and in Fig. 5 for MEAs. It is shown that all curves follow exactly the same course during a first space of time. In this period the response simply reflects the behavior of individual microband electrodes that are not influenced by perturbations from neighbouring electrodes. The corresponding trace, given as a solid line in Figs. 4 and 5, was calculated from Eq. (23) which is a simplified version of the result for a single microband electrode of width w_{el} [15]:

$$\alpha(t) = \beta(t) \approx w_{el}/\sqrt{(\pi Dt)} + 0.97. \quad (23)$$

Both the IDA and the MEA with the largest interelectrode distance follow this function during the whole time interval studied. Electrode arrays with smaller gaps evidently show an increasing deviation from the pure behavior of individual electrodes. For IDAs, the neighbourhood of oppositely polarized electrodes gives rise to an amplification of the

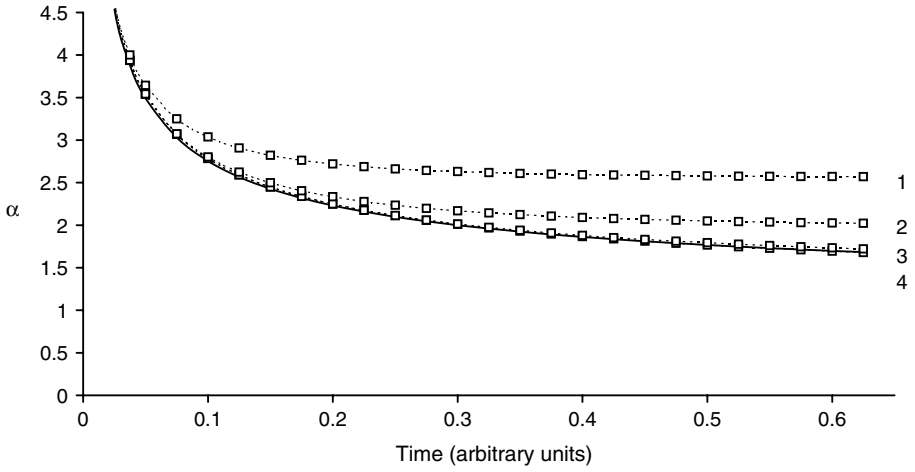

Fig. 4. Chronoamperometric response curves for different IDAs without external electrodes. Results of finite-element calculations for the current-determining factor α in Eq. (1) are given as a function of the time t, expressed in units of w_{el}^2/D. The curves 1–4 refer to IDAs with $w_g/w_{el} = 0.5$, 1, 2, and 3, respectively. The solid line shows the response of a single microband electrode according to Eq. (23). In the initial state, the whole solution contains the bulk concentrations $C_O^0 = C_R^0 = C^0$. For an electrode width of 5 μm and a diffusion coefficient of 5×10^{-6} cm^2 s^{-1}, the shown time range corresponds to 0.03 s.

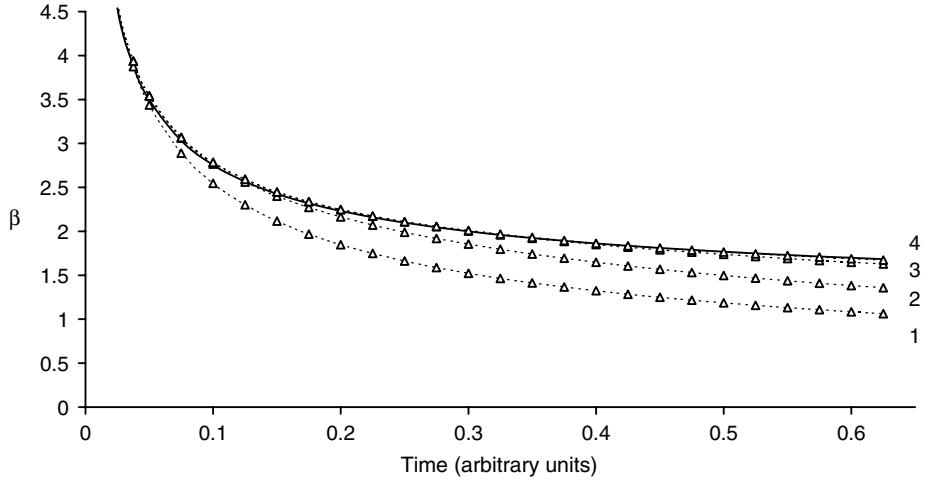

Fig. 5. Chronoamperometric response curves for different MEAs used as cathodes versus external anodes. Curves 1–4 for the factor β in Eq. (11) refer to MEAs with $w_g/w_{el} = 0.5$, 1, 2, and 3, respectively, and the solid line to a single microelectrode. The initial concentrations are $C_O^0 = C^0$ and $C_R^0 = 0$. More details are found in Fig. 4.

current (see Fig. 4). For MEAs, on the other hand, the charge flow is impeded by the presence of competing electrodes (see Fig. 5). It may be interesting to note that the lowest curve in Fig. 5 roughly fits to the time response of a 'macroelectrode' of width w for which mass transport is ideally unidimensional:

$$\beta(t) \approx w/\sqrt{(\pi Dt)}. \tag{24}$$

It is evident from Fig. 4 that IDAs reach the final current level after a time period that also depends on the gap width. The response time t_r may be defined as the interval after which the function in Eq. (23) reaches the steady-state value according to Table 1. The respective values for IDAs with $w/w_{el} = 1.5$, 2, 3, and 4 are determined as $t_r = 0.13$, 0.31, 0.95, and 2.23, given in units of w_{el}^2/D. The first two response times nicely correspond with the findings in Fig. 4. From these time intervals, the diffusion length $\sqrt{(\pi Dt)}$ after t_r is estimated as 0.6, 1.0, 1.7, and 2.7 w_{el} for the four examples of IDAs, respectively, which roughly agrees with the actual gap width.

It was shown earlier in the theoretical section that an interrelationship exists between the responses of IDAs and MEAs. At steady state, this dependence was described by Eq. (14). Very surprisingly, the same law appears to be applicable for more general cases. Fig. 6 illustrates that the validity of Eq. (14) is even maintained when the chronoamperometric response of IDAs and MEAs is considered. This finding is highly interesting and opens new possibilities for a semi-quantitative prediction of the response behavior of microband electrode arrays.

Another fundamental interrelationship between IDAs and MEAs was presented before in the context of IDAs

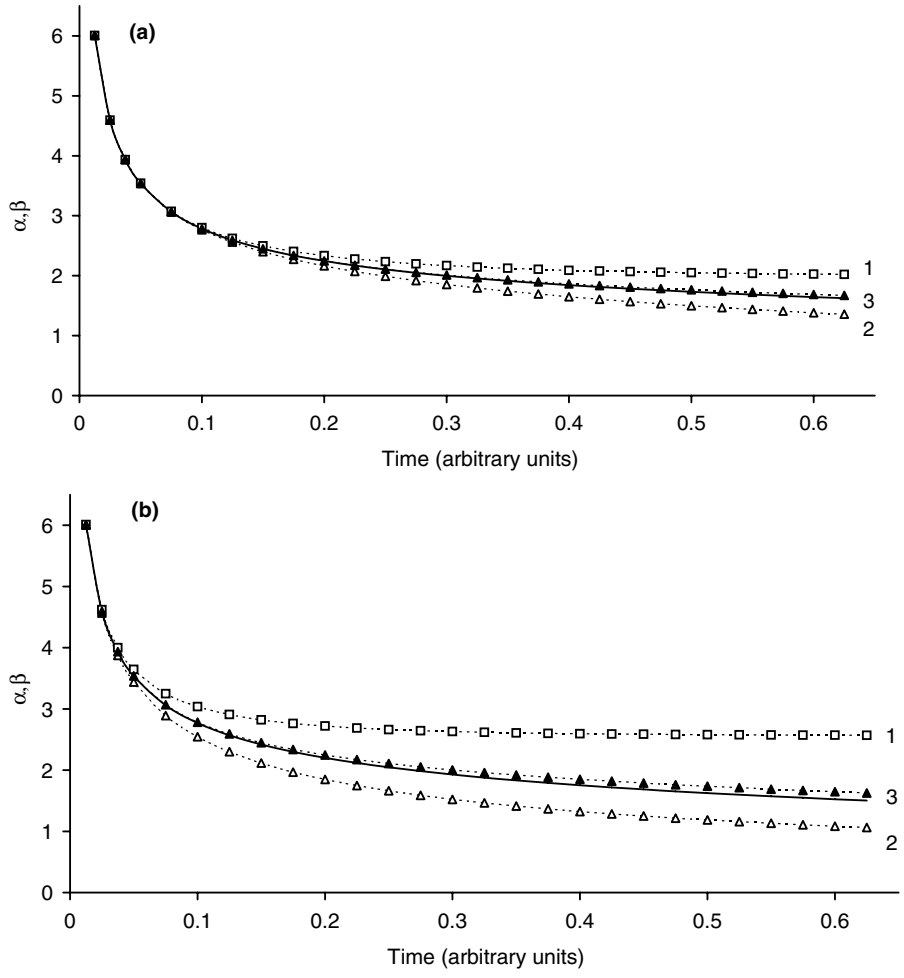

Fig. 6. Interrelationship between the current responses of IDAs and MEAs. (a) Results for an IDA with $w_g/w_{el} = 1$ (α in curve 1) and for MEAs with $w_g/w_{el} = 1$ and 3 (β in curves 2 and 3). (b) The same for an IDA with $w_g/w_{el} = 0.5$ and for MEAs with $w_g/w_{el} = 0.5$ and 2. The solid lines fitting the curves 3 are drawn according to Eq. (14) using the results from curves 1 and 2.

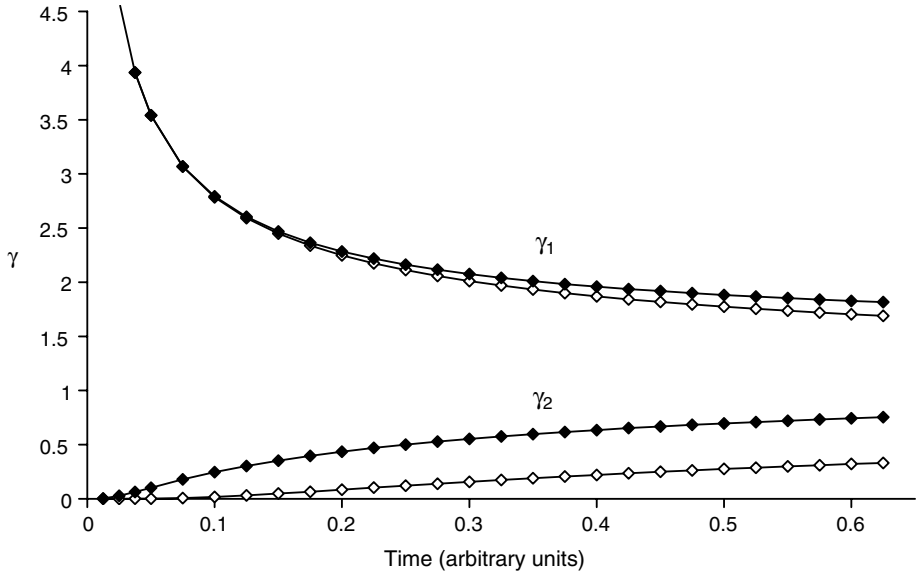

Fig. 7. Chronoamperometric responses of IDAs measured against external electrodes in a solution with $C_O^0 = C^0$ and $C_R^0 = 0$. The factors γ_1 and γ_2 in Eq. (22) for cathodic and anodic currents, respectively, are illustrated as a function of time. Results of finite-element calculations are given for IDAs with $w_g/w_{el} = 0.5$ (black symbols) and 1 (white symbols). The solid lines show the corresponding functions $0.5\,(\alpha + \beta)$ and $0.5\,(\alpha - \beta)$ obtained from Figs. 4 and 5.

that are used in measurements versus external counter electrodes. It was demonstrated that the steady-state limiting currents at cathodes and anodes, as well as the underlying concentration profiles of electroactive species, are exactly described by superimposition of the basic IDA and MEA cases. Fig. 7 clearly documents that the same principles also apply for the time-dependent response behavior of IDAs with external electrodes. The decisive factors γ_1 and γ_2, which reflect the currents at the cathodes and the anodes according to Eqs. (22a) and (22b), respectively, were determined from numerical simulations as a function of the time (data points in Fig. 7). The results indicate a similar decay of the cathodic current as in Figs. 4–6. In contrast, an increase of the anodic current is here observed since the species R are initially not present in the solution and have first to diffuse from the neighbouring cathodes. As expected, the data points for γ_1 and γ_2 can perfectly be fitted by curves calculated from the values α and β in Figs. 4 and 5 (solid lines in Fig. 7). This exact agreement finally corroborates the validity and applicability of the model description presented in this work.

4. Conclusions

New relationships for and interrelationships between the current responses of different microelectrode arrays were presented. The theoretical expressions were verified by 'experiments' performed by computer modelling. The numerical simulations made use of finite-element procedures to evaluate steady-state and time-dependent mass fluxes and concentration profiles of electroactive species at the surfaces of IDAs and MEAs. The results clearly showed that the response behavior of a given microelectrode array can be predicted either exactly or at least semi-quantitatively from the current data of other arrays. This knowledge opens new possibilities for a tailored design of IDAs and MEAs.

Appendix A. Finite-element method for numerical simulations of electrode arrays

If the electrode array is assumed to be sufficiently large, any effects resulting from the peripheral zones can be neglected. This leads to two fundamental simplifications for the modelling of the diffusion processes. First, the concentrations of electroactive species become invariant with the direction z parallel to the central axes of the array electrodes. Hence, the diffusion problem is reduced to a two-dimensional description in the x–y-plane, where the x-axis interconnects all the electrodes and the y-axis is directed from the array to the bulk solution. Second, the concentration profiles turn out to be symmetrical with respect to any y–z-plane cutting the central line of an electrode. Accordingly, such a plane can be treated as an impermeable wall, and the whole diffusion space can be subdivided in fully equivalent cells that reach from the center of a given electrode to the center of a neighbouring one. After replacing the unit cell by an x–y-network of finite elements (n,p) of the same size $\Delta x \cdot \Delta y$, the differential equations for diffusion can be replaced by:

$$J_x = -D(C_{n+1,p} - C_{n,p})/\Delta x \quad \text{(flux in } x\text{-direction)}, \tag{A.1}$$

$$J_y = -D(C_{n,p+1} - C_{n,p})/\Delta y \quad \text{(flux in } y\text{-direction)}, \tag{A.2}$$

$$\Delta C_{n,p}/\Delta t = D(C_{n+1,p} - 2C_{n,p} + C_{n-1,p})/\Delta x^2 + D(C_{n,p+1} - 2C_{n,p} + C_{n,p-1})/\Delta y^2 \quad \text{(second Fick's law)}, \tag{A.3}$$

With $\Delta x = \Delta y = \delta$, one obtains the following change of the concentration in the element (n,p) after an increase of the time by the dimensionless increment $\tau = (D/\delta^2)\Delta t$:

$$\Delta C_{n,p} = \tau \cdot (C_{n+1,p} + C_{n-1,p} + C_{n,p+1} + C_{n,p-1} - 4C_{n,p}). \tag{A.4}$$

The following boundary conditions have to be considered ($p_N\delta = \delta_N$):

$$C_{n,p=1} = C^c \text{ or } C^a \quad \text{(electrode surface)}, \tag{A.5}$$

$$C_{n,p=pN+1} = C^0 \quad \text{(bulk solution)}, \tag{A.6}$$

$$C_{n+1,p} = C_{n,p} \quad \text{(impermeable } y\text{–}z\text{-plane)}, \tag{A.7}$$

$$C_{n,p+1} = C_{n,p} \quad \text{(impermeable } x\text{–}z\text{-plane)}, \tag{A.8}$$

where Eq. (A.7) is applied for the central planes perpendicular to the electrode surfaces, and Eq. (A.8) for the boundary elements of the solution at the substrate surface between the electrodes. The total flux N_{el} (mol/s) to an electrode and the resulting current i_{el} are defined as:

$$N_{el} = -L_{el}w_{el} \cdot J_y \text{ (average at electrode)}, \tag{A.9}$$

$$i_{el} = nF \cdot N_{el}. \tag{A.10}$$

Finally, the current response can be determined as follows ($n_{el}\delta = 0.5w_{el}$):

$$i_{el} = 2nFDL_{el} \cdot \sum_{n=1}^{n_{el}} (C_{n,2} - C_{n,1}) + 2nFDL_{el} \cdot (C_{n_{el}+1,2} - C_{n_{el},1}). \tag{A.11}$$

The second term in Eq. (A.11), which has also been considered in earlier treatments [14], accounts for an additional contribution arising from radial diffusion at the edges of a microband electrode. On the other hand, lateral diffusion is neglected for all elements with $p = 1$ that are identified with the solution boundary.

To simulate the time course of concentration profiles, fluxes, and currents at IDAs and MEAs, we first choose a given initial state for the whole system of finite elements. Then, we evaluate the changes of all quantities with an increasing number of time intervals τ, until a steady state is finally reached for the studied system.

References

[1] A.J. Bard, J.A. Crayston, G.P. Kittlesen, T. Varco Shea, M.S. Wrighton, Anal. Chem. 58 (1986) 2321.

[2] B. Fosset, Ch. Amatore, J.E. Bartelt, R.M. Wightman, Anal. Chem. 63 (1991) 306.
[3] B. Fosset, Ch. Amatore, J.E. Bartelt, R.M. Wightman, Anal. Chem. 63 (1991) 1403.
[4] H. Rajantie, J. Strutwolf, D.E. Williams, J. Electroanal. Chem. 500 (2001) 108.
[5] I.B. Svir, A.I. Oleinick, R.G. Compton, J. Electroanal. Chem. 560 (2003) 117.
[6] Ch. Amatore, M. Belotti, Y. Chen, E. Roy, C. Sella, L. Thouin, J. Electroanal. Chem. 573 (2004) 333.
[7] K. Aoki, M. Morita, O. Niwa, H. Tabei, J. Electroanal. Chem. 256 (1988) 269.
[8] D.G. Sanderson, L.B. Anderson, Anal. Chem. 57 (1985) 2388.
[9] O. Niwa, M. Morita, H. Tabei, Anal. Chem. 62 (1990) 447.
[10] O. Niwa, M. Morita, H. Tabei, J. Electroanal. Chem. 267 (1989) 291.
[11] M. Morita, O. Niwa, T. Horiuchi, Electrochim. Acta 42 (1997) 3177.
[12] M. Paeschke, U. Wollenberger, T. Lisec, U. Schnakenberg, R. Hintsche, Sensors Actuators B 26–27 (1995) 394.
[13] F. Björefors, C. Strandman, L. Nyholm, Electroanalysis 12 (2000) 255.
[14] K. Aoki, M. Tanaka, J. Electroanal. Chem. 266 (1989) 11.
[15] K. Aoki, K. Tokuda, H. Matsuda, J. Electroanal. Chem. 230 (1987) 61.
[16] W.E. Morf, Anal. Chim. Acta 330 (1996) 139.
[17] A.J. Bard, L.R. Faulkner, Electrochemical Methods, Fundamentals and Applications, Wiley, New York, 1980.
[18] J. Crank, The Mathematics of Diffusion, second ed., Oxford University Press, Oxford, 1975.